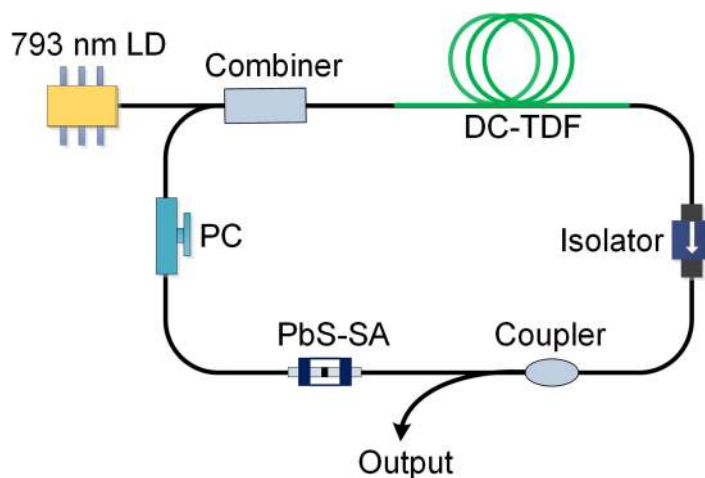# Lead Sulfide Saturable Absorber Based Passively Mode-Locked Tm-Doped Fiber Laser

Fei Liu
Ying Zhang
Xiaodong Wu
Jianfeng Li, *Senior Member, IEEE*
Fei Yan
Xiaohui Li
Abdul Qyyum
Zhu Hu
Chen Zhu
Yong Liu, *Senior Member, IEEE*

Lead Sulfide Saturable Absorber Based Passively Mode-Locked Tm-Doped Fiber Laser

Fei Liu,[1] **Ying Zhang,**[2] **Xiaodong Wu,**[1]
Jianfeng Li ⓘ **,**[1] *Senior Member, IEEE***, Fei Yan,**[1]
Xiaohui Li ⓘ **,**[2] **Abdul Qyyum,**[2] **Zhu Hu,**[1] **Chen Zhu,**[3]
and Yong Liu,[1] *Senior Member, IEEE*

[1]State Key Laboratory of Electronic Thin Films and Integrated Devices, School of Optoelectronic Science and Engineering, The University of Electronic Science and Technology of China (UESTC), Chengdu 610054, China
[2]School of Physics and Information Technology, Shaanxi Normal University, Xi'an 710119, China
[3]Science and Technology on Solid-State Laser Laboratory, Beijing 100015, China

Abstract: In this paper, a passively mode-locked Tm-doped fiber laser by employing lead sulfide (PbS) nanoparticles as the saturable absorber (SA) is successfully demonstrated in the 2 μm region for the first time, to the best of our knowledge. Measured by a home-made balanced twin-detector setup at 2 μm, the PbS SA was characterized by the modulation depth of 10.69%, the non-saturable loss of 74.27%, and the saturable peak intensity of 8.62 MW/cm^2, respectively. The laser delivered stable conventional soliton with a pulse duration of 1.24 ps and a repetition rate of 21.93 MHz. The center wavelength and 3 dB bandwidth are 1957.37 nm and 3.43 nm, respectively. Additionally, the second-order harmonic soliton pulses with a repetition rate of 43.86 MHz were also observed by further increasing the pump power. Our work reveals that PbS material is a reliable SA applied for pulse generation in the 2 μm spectral region.

Index Terms: Tm-doped fiber laser, lead sulfide, saturable absorber, mode-locking.

1. Introduction

In recent years, 2 μm mode-locked Tm-doped fiber lasers have attracted much attention owing to its unique applied advantages in mid-infrared wavelength conversion, medical diagnosis, laser LIDAR, nanoscale imaging, special material processing and so on [1]–[7]. A key point for the formation of mode-locking is the saturable absorption effect, which can be achieved using either artificial SAs based on fiber's nonlinear Kerr effect or real SAs based on the nonlinear absorption effect [8]–[10]. However, the former usually needs strong pump strength and long cavity length due to the high nonlinear threshold of silica fiber, which inevitably leads to bulky construction

and is not conducive to realize the self-starting of mode-locking [11], [12]. Therefore, the real SAs with a low response threshold are alternatively adopted to achieve mode-locking. In the past few decades, semiconductor saturable absorber mirrors (SESAMs) [13]–[15] have been regarded as one of the most important elements for mode-locking. However, it usually requires complex fabrication process and costly systems. Nowadays, a series of low dimensional SAs including CNTs [16]–[18], graphene [12], [19]–[21], transition metal dichalcogenides (TMDCs) (e.g., WS_2, MoS_2, WSe_2, $MoSe_2$ and ReS_2) [22]–[27] and black phosphorus [28]–[31] have been regarded as good substitutes for SESAMs. These SAs have been widely used to achieve mode-locking at different optical bands. Among them, CNTs are widely adopted because of its good stability and fast response time. Especially, Liu *et al.* revealed the dynamics buildup process of soliton molecules, harmonic mode-locking states, and the transition from Q-Switching to mode-locking in a CNT SA based ultrafast fiber laser [32]–[34], providing the theoretical and experimental basis for the researchers to better understand the soliton dynamics in the fiber laser. Nevertheless, the accurate control of CNT's diameter is required to match the desired laser wavelengths with the absorption, which restricts its broadband tunability. Although graphene possesses an excellent broadband absorption performance as a result of its zero bandgap, suitable modulation depth for pulse generation cannot be ensured due to the weak absorption of approximately 2.3% per layer. Owing to the unique absorption, TMDCs have been also employed to achieve pulsed fiber laser in the visible spectral range. But large direct bandgaps of TMDCs result in that suitable defects should be introduced to extend laser wavelengths, which increases their fabricating complexity and limits their application in mid-infrared region. In contrast, black phosphorus as an emerging SA in recent years, offers a layer-dependent bandgap from 0.3 (bulk) to 2 eV (monolayer), widely covering the bandgap range of graphene and TMDCs. Unfortunately, it is easily oxidized and has a bad stability.

Most recently, semiconductor PbS nanoparticles as the oldest light-harvesting materials for infrared detectors [35], biomarkers [36], [37] and solar cells [38], [39], presented its great optical potential from near-infrared to mid-infrared region (1~3.2 μm) [40], [41]. Owing to its narrow bandgap (0.41 eV), bandgap tunability and good long-term stability, PbS nanoparticles have attracted people's intensive attention and been regarded as an effective SA material to overcome the shortcomings of the aforementioned materials. Lee *et al.* demonstrated a 1.55 μm passively Q-switched erbium-doped fiber laser by using the film-type PbS quantum dots (QDs) material as the SA [42]. After that, based on the PbS/CdS core/shell QDs SA, Ming *et al.* obtained the mode-locked Er-doped fiber laser with 54 ps pulse duration and 2.71 mW maximal output power [43]. Then, at the same waveband, the PbS QDs in polystyrene films was fabricated to realize the Q-switched Er-doped fiber laser by Sun *et al.* This fiber laser yielded stable Q-switched pulses with maximum output power of 40.19 mW and pulse duration of 3.9 μs [44]. Due to the polymer films structure, however, these PbS QDs as SAs have low damage threshold and consequently limits the performance of mode-locking. By employing the PbS nanoparticles without any polymer as the SA, Zhang *et al.* have obtained a 1533 nm mode-locked fiber laser with good stability for more than 1 month, which proved the potential of PbS nanomaterials in ultra-short pulse generation [45]. Furthermore, using the same PbS nanoparticles, our research group has successfully demonstrated the Q-switched Dy^{3+}-doped fiber laser that is tunable from 2.71 to 3.08 μm [46]. Although these works indicate that PbS material as the SA is a good candidate for the fiber lasers at 1.5 μm and 3 μm wavelength range, it has never been reported in the 2 μm region.

In our work, we experimentally demonstrated a stable 2 μm passively mode-locked Tm-doped fiber laser using PbS nanomaterials as the SA. The nonlinear characteristics of PbS were measured by a 2 μm home-made mode-locked fiber laser. The fiber laser mode-locked by PbS SA delivered stable conventional soliton pulses operating at fundamental repetition rate state. When further increasing pump power, a second-order harmonic mode-locking was also obtained.

2. Preparation and Characterization of PbS SA

In our experiment, the PbS sample was prepared by using the sol-gel method and mixing PbS powder with acetone solvent in a volume ratio of 1:3. Stable PbS nanoparticles dispersion was
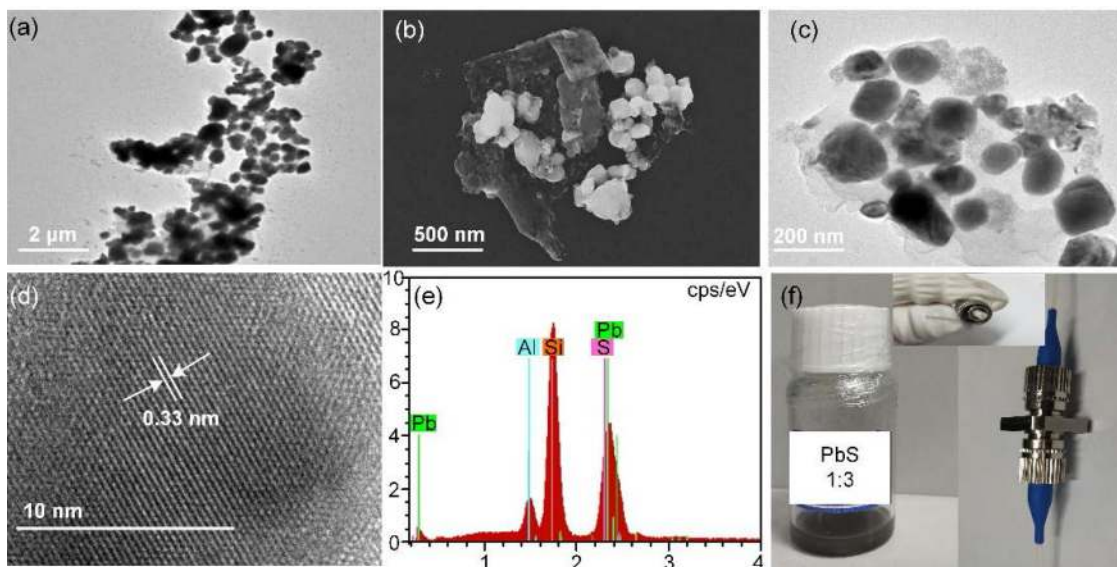
Fig. 1. Characterization of PbS nanoparticles dispersion. (a) The SEM image with 2 μm scale. (b) The SEM image with 500 nm scale. (c) The TEM image with 200 nm scale. (d) The HRTEM (high-resolution TEM) image with 10 nm scale. (e) The EDS analysis. (f) Photograph of PbS nanoparticles dispersion and the fiber-compatible PbS-SA device.

collected from the supernatant after centrifugation to separating large agglomerations for 30 minutes at 2000 rpm in a vortex mixer (Langyue SK-1, China). For the PbS nanoparticles dispersion, the scanning electron microscopy (SEM: Hitachi SU8220, Japan) images with different scales (2 μm and 500 nm) are shown in Figs. 1(a) and 1(b). It is seen that PbS nanoparticles obviously present irregular microstructure, mainly existing in the forms of stereo-structure and polygon. Feng *et al*. explained the reason why the irregular shapes of PbS nanoparticles formed [47]. In Fig. 1(c), the transmission electron microscopy (TEM: JEOL JEM-2100, Japan) image provides that the lateral size of PbS nanoparticles is in the range of 75–200 nm. The measured average size of individual PbS nanoparticle is approximately 80 nm. Note that some of the larger and the darker nanoparticles were generated by the agglomeration of smaller particles [48], [49]. Thus, the size distribution of PbS nanoparticles is not as broad as we can see. Fig. 1(d) presents a high resolution TEM (HRTEM: JEOL JEM-2100, Japan) image with 10 nm lateral size. The observed spacing of lattice fringes is approximately 0.33 nm. A clear cladding was formed by acetone attached solution during the fabrication process of PbS nanoparticles dispersion, which reveals a signal of good dispersibility. As illustrated in Fig. 1(e), the energy dispersive spectroscopy (EDS) analysis of PbS nanoparticles was also executed. It is seen that the chemical composition of the sample corresponds well to the atomic structure of PbS, except for Si and Al derived from the sample placement stations. To further confirm the pulse generation performance of PbS nanoparticles dispersion, it was deposited on the end face of fiber jumper (shown in the inset of Fig. 1(f)) and then was fabricated as a fiber-compatible SA.

Additionally, we designed a typical balanced twin-detector setup to investigate the nonlinear transmission characteristics of PbS SA in the experiment, as depicted in Fig. 2(a). The home-made 2 μm all-fiber pulse laser source consists of a picosecond Tm-doped fiber laser seed and a Tm-doped fiber amplifier. For the amplified picosecond pulse with a maximum average power of 39.6 mW, its repetition rate, pulse duration, and signal-to-noise ratio (SNR) are 10.27 MHz, 21 ps, and 60.5 dB, respectively. The laser output was divided into a reference path and a measurement path using a 3-dB optical coupler. To minimize the measuring errors, the average output powers of two optical paths were detected using the same model power meters with the measurement accuracy of microwatt level. Fig. 2(b) presents the nonlinear transmission curve of PbS SA by
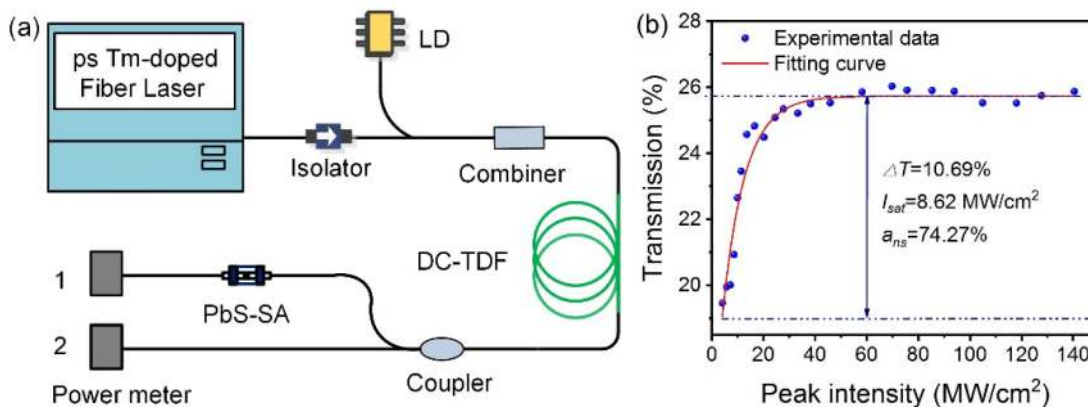
Fig. 2. (a) The experimental setup for the nonlinear transmission measurement of PbS SA. (b) Measured nonlinear transmission curves.
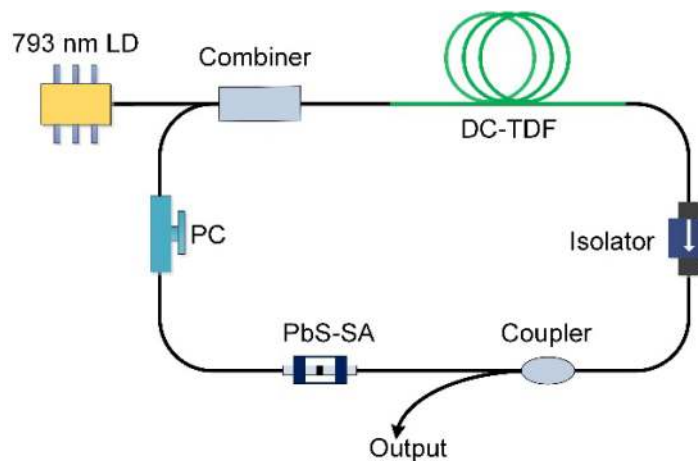

Fig. 3. Setup of passively mode-locked Tm-doped fiber laser based on PbS SA.

fitting the measured data with the following formula [23]:

$$T(I) = 1 - \Delta T \times \exp(-I/I_{sat}) - \alpha_{ns}, \tag{1}$$

where $T(I)$ is the transmittance and I is the incident peak intensity. ΔT, α_{ns} and I_{sat} represent the modulation depth, the non-saturable loss and the saturable peak intensity of PbS SA, which are calculated to be 10.69%, 74.27%, and 8.62 MW/cm^2, respectively.

3. Experiment Setup

The experimental ring configuration of the Tm-doped fiber laser is presented in Fig. 3. With a $(2 + 1)$ $\times 1$ pump combiner (ITF, Canada), a commercial multimode 793 nm laser diode (BWT, China) was utilized as pump source to supply outside energy for the laser oscillator. A 1.1 m Tm-doped double-cladding fiber (Coractive-DCF-TM-10/128) was served as the gain fiber. Tm-doped fiber is characterized by an octagonal shaped inner cladding with 0.45 numerical aperture (NA) and the circular fiber core with 0.22 NA. A polarization-independent isolator (Advanced Photonics, USA) ensured laser's unidirectional operation. 10% of a 9:1 optical coupler (OC) (AdValue Photonics, USA) was utilized to output the laser. A polarization controller (PC) was used to optimize the
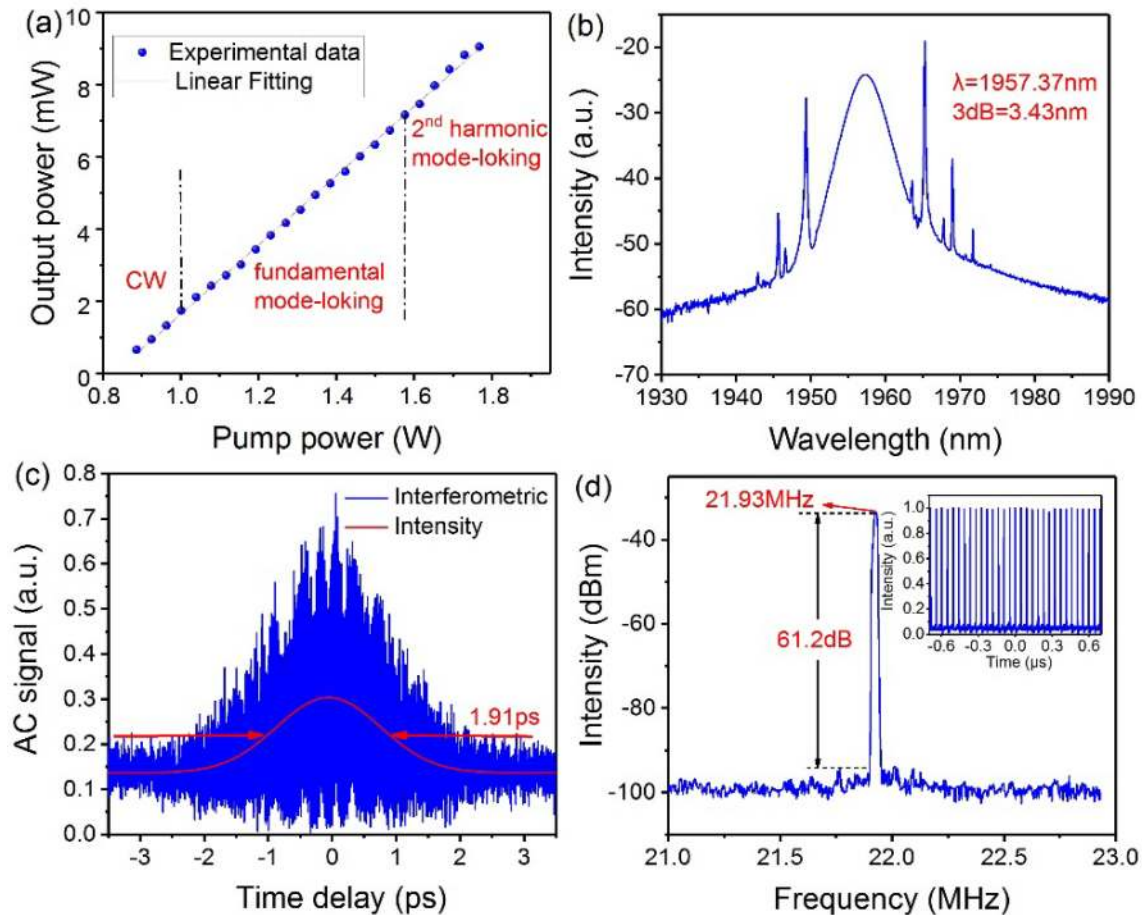
Fig. 4. (a) Output power as a function of pump power. (b) Soliton optical spectrum. (c) Pulse autocorrelation with sech^2 fitting. (d) RF spectrum with the resolution bandwidth of 3 kHz and the scanning range of 2 MHz. Inset: Oscilloscope trace.

performance of mode-locking. PbS SA was positioned between the OC and PC. The total laser cavity length is 9.43 m, including 1.1 m TDF and 8.33 m SMF28e tail fibers of the intra-cavity fiber components. The anomalous dispersion values of these two fibers at 1.993 μm ware about -84 ps^2/km and -80 ps^2/km, respectively [50]. The estimated value of net cavity dispersion is -0.75 ps^2. In order to obtain the laser signal, an optical spectrum analyzer (Yokogawa AQ6375, Japan) with a high resolution of 0.05 nm and an interference autocorrelator (APE Pulsecheck, Germany) were respectively applied for the real-time measurement of optical spectrum and pulse duration. In addition, a 2-μm InGaAs photodetector (EOT ET-5000F, USA) with a bandwidth of 12.5 GHz and a response time of 28 ps was employed to detect the radio-frequency (RF) spectrum and oscilloscope trace.

4. Experiment Results and Discussion

In the experiment, once the PC's position was properly set, stable mode-locking was self-started by simply increasing the pump power. Fig. 4(a) presents the relationship between pump power and output power, as well as the operation state of the passively mode-locked Tm-doped fiber oscillator. Continuous wave (CW) with the output power of 0.66 mW firstly appeared at the pump

power of 0.88 W. When the pump power was increased to 1.01 W, the laser switched into the mode-locking regime. Conventional soliton with a maximum output power of 6.34 mW was obtained at the pump power of 1.54 W. A segment of double-cladding single-mode Thulium-doped fiber (DC-SM-TDF) was adopted in our work is the reason why the pump threshold of the mode-locking is up to ~1 W. We can further improve the output power by optimizing the parameter performance of PbS SA (such as the deposition thickness and the size of nanoparticles), and decreasing the intra-cavity loss. Additionally, using a linear cavity mode-locking structure based on PbS SA is also a good method to realize the higher power ultrashort pulse laser output. Fig. 4(b) shows the corresponding optical spectrum of conventional soliton. Its center wavelength and 3 dB bandwidth are 1957.37 nm and 3.43 nm, respectively. A series of Kelly sidebands symmetrically distributed around the main peak is a good indication of the conventional soliton operation, which is caused by the spectral interference of dispersive waves. Some sub-sidebands caused by the four-wave mixing (FWM) between the orthogonal soliton components in the fiber laser [51], also can be observed on the mode-locked spectrum. Fig. 4(c) shows the measured interference and intensity autocorrelation trace with a 7-ps scanning range. Autocorrelation signal with a full width at half maximum (FWHM) of 1.91 ps was fitted by using the sech^2 function, corresponding to a pulse duration of 1.24 ps. Thus, the calculated time-bandwidth product (TBP) of 0.335 indicates that the mode-locking is almost transform-limited. In Fig. 4(d), the RF spectrum with a resolution bandwidth of 3 kHz and a scanning range of 2 MHz shows a high signal-noise ratio of 61.2 dB, which suggests the good uniformity of the pulse train. The measured repetition rate of 21.93 MHz is in agreement with the theoretical cavity length dependent value, implying that single pulse was obtained per round trip. The pulse train with the amplitude fluctuation of less than 0.8% is illustrated in the inset of Fig. 4(d), which exhibits the good stability of the passive mode-locked fiber laser based on PbS SA.

The above single soliton state maintained at the pump range from 1.01 W to 1.54 W. When pump power exceeded 1.54 W, the multi-pulses appeared. By appropriately adjusting the pump power and the PC's position, the multi-pulses operated at the 2nd-order harmonic state. Fig. 5 shows an example of this state at the pump power of 1.77 W. The spectrum is presented in Fig. 5(a), showing a 3-dB bandwidth of 4.22 nm visibly wider than previous fundamental frequency soliton. It is seen from the inset of Fig. 5(b) that the spectrum peak intensity monotonously decreases with increased order of the RF spectrum component, and the separation between two adjacent spectrum components always keeps constant, suggesting the high uniformity of the 2nd harmonic pulse train. The high signal noise ratio of 60.26 dB also indicates its good stability for pulse generation. Moreover, the RF spectrum with a scanning range of 1 MHz and a resolution bandwidth of 3 kHz was measured to investigate the quality of the 2nd harmonic soliton pulses. In Fig. 5(c), the measured oscilloscope trace shows that a stable pulse train uniformly exists with constant pulse separation of 22.8 ns, corresponding to the pulse repetition rate of 43.86 MHz. This is twice of the fundamental repetition rate of the laser cavity, indicating the 2nd-order harmonic operation. Fig. 5(d) shows the measured autocorrelation trace with sech^2 fitting in a 5-ps scan range. According to the FWHM of 1.682 ps when sech^2-pulse fit is assumed, the pulse duration of harmonic mode-locking (HML) pulse is estimated to be 1.09 ps. The calculated TBP of 0.36 implies that the pulse is slightly chirped. The average output power is 9.06 mW corresponding to the pulse energy of 206.8 pJ. Note that it is difficult to further increase the harmonic order in our experiment, due to the high soliton splitting threshold in the large anomalous dispersion region determined by the soliton area theorem [52], [53]. By reducing the net anomalous cavity dispersion or inducing high-nonlinear component to reduce the soliton splitting threshold inside the laser cavity, the higher order harmonic or noise-like pulse could be realized. Until the maximum pump power of 1.77 W, the mode-locking is still observed, suggesting that PbS SA is undamaged. According to the intra-cavity laser intensity of 90.6 mW at stable mode-locking operation, the peak power density in the fiber laser is estimated to be 360 MW/cm^2, revealing that the PbS SA has a damage threshold higher than this value. In addition, the mode-locked fiber laser could stably operate for more than half a month without any deterioration, which shows its good long-term stability. Note that no Q-switching was observed due
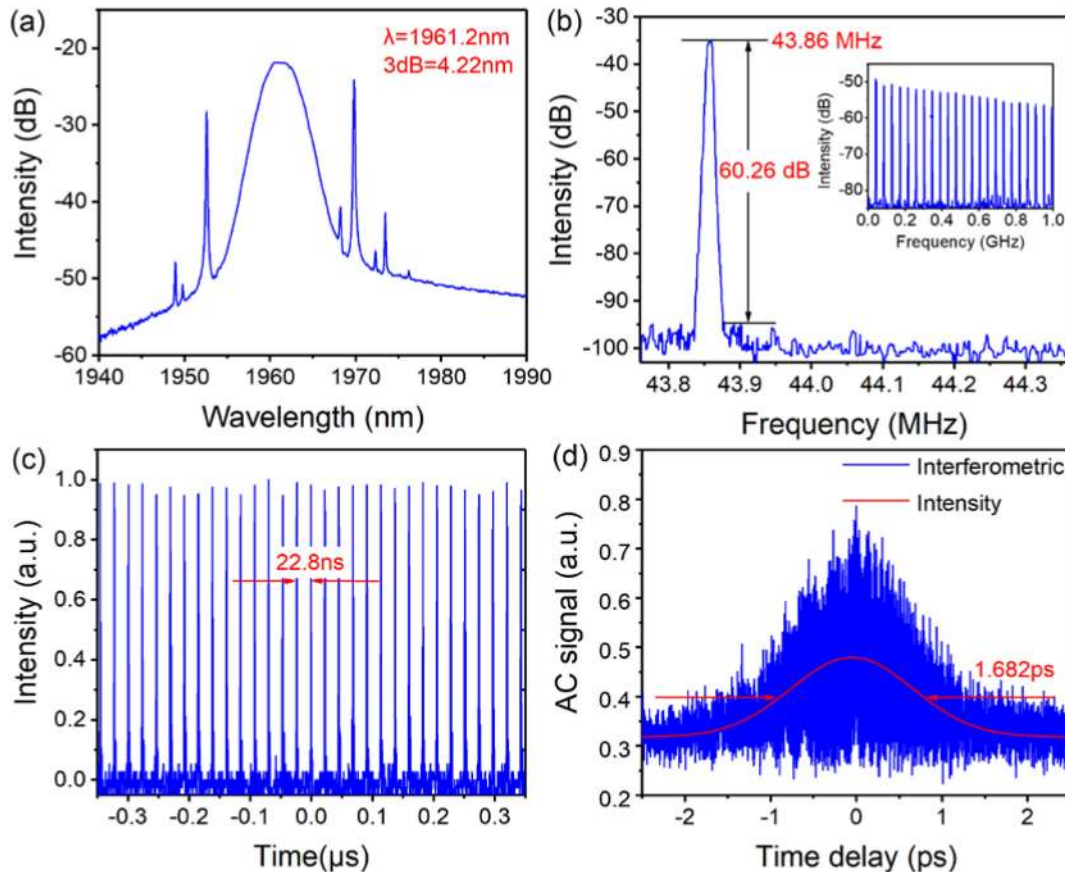
Fig. 5. The second-order harmonic mode-locking pulse at the pump power of 1.77 W. (a) The optical spectrum. (b) RF spectrum with the 3 kHz resolution bandwidth and 2 MHz scanning range, inset: RF spectrum with a scanning range of 1.0 GHz. (c) Oscilloscope trace. (d) Pulse autocorrelation with sech^2 fitting in a 5-ps scan range.

to low intra-cavity energy loss and a modulation depth (10.69%) capable of achieving mode-locking. Many similar phenomena have been reported in graphene, carbon-nanotube, or alcohol based pulse fiber lasers [54]–[58]. A key factor to realize the Q-switching operation is controlling the loss of the oscillator. Thus, the Q-switched pulse can be achieved by adjusting the parameters of PbS SA or changing the operating condition of this oscillator. For the SA material, we can prepare the PbS SA with a higher modulation depth and saturable peak intensity to increase the pump threshold of fiber laser. Meanwhile, by changing the splitting ratio of optical coupler from 9/1 to 5/5, the Q-switched state can also be generated in the PbS SA based Tm-doped fiber laser due to the higher intra-cavity loss. To indicate the unique advantages of PbS SA based mode-locking fiber laser, the mode-locked fiber lasers with PbS SA and other different SAs were compared in Table 1. It can be seen that PbS SA has a higher modulation depth appropriate for the mode-locking pulse generation. Moreover, the temporal pulse width of our fiber laser is almost comparable to those from the lasers using graphene and TMDCs, and it is shorter than the laser output using CNT or SESAM. The results suggest that PbS nanoparticles dispersion can be regarded as an effective saturable absorber for ultra-short pulse generation in the Tm-doped fiber laser. This also provides us for a reliable ultra-short pulse source to realize the nonlinear mid-infrared light generation in the future work.

TABLE 1

The Comparison of 2 μm Tm-Doped Fiber Lasers Mode-Locked With Different SA Materials

Saturable Absoption Materials	Modulation Depth @ 2 μm	Non-saturable Loss @ 2 μm	Pulse Wavelength (nm)	Output Spectral Bandwidth (nm)	Output Pulse Width (ps)	References
SWCNT	-	-	1944	0.45	10	[59]
graphene	-	-	1940	2.1	3.6	[20]
graphene	-	-	1901.6	1.5	0.37	[60]
graphene	-	-	1944	3.9	0.933	[61]
graphene	<0.8%	-	1884	4	1.2	[62]
graphene	~2.7%	-	1912-1918	0.26@1908nm	6500	[63]
graphene	-	-	1953	2.2	2.1	[64]
SESAM	-	-	1980	92	1.5	[13]
SESAM	20%	16%	1962	0.37	18	[14]
SESAM	26%	-	1978	2	815	[15]
SESAM	20%	16%	1945	6.1	0.7	[65]
WS$_2$	~10.9%	38.4%	1925	5.6	~1.3	[66]
MoS$_2$	13.6	16.7%	1940	~17.3	843	[23]
MoS$_2$	12.5%	27.2%	1927	2.86	1.51	[67]
MoSe$_2$	4.4%	45.5%	1912.6	4.62	0.92	[68]
WSe$_2$	1.83%	87%	1863.96	3.19	1.16	[69]
MoTe$_2$	5.7%	70%	1930.22	4.45	0.952	[70]
PbS	10.69%	74.27%	1957.37 / 1961.2	3.43 / 4.22	1.24 / 1.09	This work

5. Conclusion

In summary, PbS nanoparticles dispersion was successfully employed as SA to achieve a passively mode-locked Tm-doped fiber laser. Nonlinear saturable absorption properties of the PbS nanoparticles dispersion were also measured in the 2 μm spectral region, by using the homemade measurement setup in our experiment. PbS SA has the measured modulation depth of 10.69%, non-saturable loss of 74.27% and saturation peak intensity of 8.62 MW/cm^2. When the laser operated at the stable fundamental frequency mode-locked state, the pulse duration was measured to be 1.24 ps. In addition, by further increasing the pump power, the mode-locking switches into the second-order harmonic regime with the repetition rate of 43.86 MHz and the SNR of 60.26 dB. These results suggest that PbS nanoparticles dispersion could be developed as an effective SA material for 2 μm mode-locking generation.

Acknowledgment to Author Contribution

References

[1] I. T. Sorokina, V. V. Dvoyrin, N. Tolstik, and E. Sorokin, "Mid-IR ultrashort pulsed fiber-based lasers," *IEEE J. Sel. Top. Quant. Electron.*, vol. 20, no. 5, pp. 99–110, 2014.
[2] K. Scholle, S. Lamrini, P. Koopmann, and P. Fuhrberg, "2 μm laser sources and their possible applications," in *Frontiers in Guided Wave Optics and Optoelectronics*, B. Pal, ed., London: IntechOpen, pp. 471–500, 2010.
[3] K. Yin, B. Zhang, G. Xue, L. Li, J. Hou, "High-power all-fiber wavelength-tunable thulium doped fiber laser at 2 μm," *Opt. Express*, vol. 22, no. 17, pp. 19947–19952, 2014.
[4] M. Jung *et al.*, "A femtosecond pulse fiber laser at 1935 nm using a bulk-structured Bi$_2$Te$_3$ topological insulator," *Opt. Express*, vol. 22, no. 1935, pp. 7865–7874, 2014.
[5] D. Mao *et al.*, "Soliton fiber laser mode locked with two types of film-based Bi$_2$Te$_3$ saturable absorbers," *Photon. Res.*, vol. 3, pp. A43–A46, 2015.

[6] W. Yang, B. Zhang, J. Hou, K. Yin, and Z. Liu, "A novel 2-μm pulsed fiber laser based on a supercontinuum source and its application to mid-infrared supercontinuum generation," *Chin. Phys. B*, vol. 23, pp. 1–7, 2014, Art. no. 054208.

[7] K. Yin, B. Zhang, L. Y. Yang, and J. Hou, "15.2 W spectrally flat all-fiber supercontinuum laser source with >1 W power beyond 3.8 μm," *Opt. Lett.*, vol. 42, no. 12, pp 2334–2337, 2017.

[8] X. Wang, P. Zhou, X. Wang, H. Xiao, and Z. Liu, "Pulse bundles and passive harmonic mode-locked pulses in Tm-doped fiber laser based on nonlinear polarization rotation," *Opt. Express*, vol. 22, no. 5, pp. 6147–6153, 2014.

[9] C. W. Rudy, K. E. Urbanek, M. J. F. Digonnet, and R. L. Byer, "Amplified 2-μm thulium-doped all-fiber mode-locked figure-eight laser," *J. Lightw. Technol.*, vol. 31, no. 11, pp. 1809–1812, 2013.

[10] J. Li *et al.*, "All-fiber passively mode-locked Tm-doped NOLM-based oscillator operating at 2-μm in both soliton and noisy-pulse regimes," *Opt. Express*, vol. 22, no. 7, pp. 7875–7882, 2014.

[11] R. C. Sharp, D. E. Spock, N. Pan, and J. Elliot, "190-fs passively mode-locked thulium fiber laser with a low threshold," *Opt. Lett.*, vol. 21, no. 12, pp. 881–883, 1996.

[12] J. Sotor *et al.*, "All-fiber Ho-doped mode-locked oscillator based on a graphene saturable absorber," *Opt. Lett.*, vol. 41, no. 11, pp. 2592–2505, 2016.

[13] Q. Wang, J. Geng, T. Luo, and S. Jiang, "Mode-locked 2 μm laser with highly thulium-doped silicate fiber," *Opt. Lett.*, vol. 34, no. 23, pp. 3616–3618, 2009.

[14] J. Liu, Q. Wang, and P. Wang, "High average power picosecond pulse generation from a thulium-doped all-fiber MOPA system," *Opt. Express*, vol. 20, no. 20, pp. 22442–22447, 2012.

[15] W. Zhou, D. Y. Shen, Y. S. Wang, J. Y. Long, and Y. An, "Mode-locked thulium-doped fiber laser with a narrow bandwidth and high pulse energy," *Laser Phys. Lett.*, vol. 9, no. 8, pp. 587–590, 2012.

[16] M. A. Chernysheva, A. A. Krylov, N. R. Arutyunyan, A. S. Pozharov, E. D. Obraztsova, and E. M. Dianov, "SESAM and SWCNT mode-locked all-fiber thulium-doped lasers based on the nonlinear amplifying loop mirror," *IEEE J. Sel. Top. Quant. Electron.*, vol. 20, no. 5, pp. 448–455, 2014, Art. no. 1101208.

[17] K. Keiu and F. W. Wise, "Soliton thulium-doped fiber laser with carbon nanotube saturable absorber," *IEEE Photon. Technol. Lett.*, vol. 21, no. 3, pp. 128–130, 2009.

[18] G. Sobon, A. Duzynska, M. Świniarski, J. Judek, J. Sotor, and M. Zdrojek, "CNT-based saturable absorbers with scalable modulation depth for Thulium-doped fiber lasers operating at 1.9 μm," *Sci. Rep.*, vol. 7, pp. 1–9, 2017, Art. no. 45491.

[19] W. D. Tan, C. Y. Su, R. J. Knize, G. Q. Xie, L. J. Li, and D. Y. Tang, "Mode locking of ceramic Nd: Yttrium aluminum garnet with graphene as a saturable absorber," *Appl. Phys. Lett.*, vol. 96, no. 3, pp. 1–4, 2010, Art. no. 031106.

[20] M. Zhang *et al.*, "Tm-doped fiber laser mode-locked by graphene-polymer composite," *Opt. Express*, vol. 20, no. 22, pp. 25077–25084, 2012.

[21] J. Sotor, I. Pasternak, A. Krajewska, W. Strupinski, and G. Sobon, "Sub-90 fs a stretched-pulse mode-locked fiber laser based on a graphene saturable absorber," *Opt. Express*, vol. 23, no. 21, pp. 27503–27508, 2015.

[22] B. Guo, Q. Lyu, Y. Yao, and P. F. Wang, "Direct generation of dip-type sidebands from WS_2 mode-locked fiber laser," *Opt. Mater. Express*, vol. 6, no. 8, pp. 2475–2486, 2016.

[23] T. Zhen *et al.*, "Mode-locked thulium fiber laser with MoS_2," *Laser Phys. Lett.*, vol. 12, no. 6, 2015, pp. 1–5, Art. no. 065104.

[24] J. Zhang *et al.*, "Ultrafast saturable absorption of MoS_2 nanosheets under different pulse-width excitation conditions," *Opt. Lett.*, vol. 43, no. 2, pp. 243–246, 2018.

[25] J. Wang *et al.*, "Ultrafast thulium-doped fiber laser mode locked by monolayer WSe_2," *IEEE J. Sel. Top. Quant. Electron.*, vol. 24, no. 3, pp. 1–6, May-Jun. 2018, Art. no. 1100706.

[26] R.I. Woodward *et al.*, "Wideband saturable absorption in few-layer molybdenum diselenide ($MoSe_2$) for Q-switching Yb-, Er- and Tm-doped fiber lasers," *Opt. Express*, vol. 23, no. 15, pp. 20051–20061, 2015.

[27] D. Mao *et al.*, "Passively Q-switched and mode-locked fiber laser based on an ReS_2 saturable absorber," *IEEE J. Sel. Top. Quant. Electron.*, vol. 24, no. 3, pp. 1–6, May-Jun. 2018, Art. no. 1100406.

[28] Y. Chen *et al.*, "Mechanically exfoliated black phosphorus as a new saturable absorber for both Q-switching and mode-locking laser operation," *Opt. Express*, vol. 23, no. 10, pp. 12823–12833, 2015.

[29] J. Sotor, G. Sobon, M. Kowalczyk, W. Macherzynski, P. Paletko, and K. M. Abramski, "Ultrafast thulium-doped fiber laser mode locked with black phosphorus," *Opt. Lett.*, vol. 40, no. 16, pp. 3885–3888, 2015.

[30] K. Wu *et al.*, "High performance mode-locked and Q-switched fiber lasers based on novel 2D materials of topological insulators, transition metal dichalcogenides and black phosphorus: Review and perspective (invited)," *Opt. Commun.*, vol. 406, pp. 214–229, 2018.

[31] H. Yu, X. Zheng, K. Yin, X. Cheng, and T. Jiang, "Thulium/holmium-doped fiber laser passively mode locked by black phosphorus nanoplatelets-based saturable absorber," *Appl. Optics*, vol. 54, no. 34, pp. 10290–10294, 2015.

[32] X. M. Liu, X. K. Yao, and Y. D. Cui, "Real-time observation of the buildup of soliton molecules," *Phys. Rev. Lett.*, vol. 121, pp. 1–6, 2018, Art. no. 023905.

[33] X. M. Liu, D. Popa, and N. Akhmediev, "Revealing the transition dynamics from Q-Switching to mode-locking in a soliton laser," *Phys. Rev. Lett.*, vol. 123, pp. 1–6, 2019, Art. no. 093901.

[34] X. M. Liu, and M. Pang, "Revealing the buildup dynamics of harmonic mode-locking states in ultrafast lasers," *Laser Photon. Rev.*, vol. 13, 2019, Art. no. 1800333.

[35] M. Li, Q. Wang, X. Shi, L. A. Hornak, and N. Wu, "Detection of mercury (II) by quantum dot/DNA/goldnanoparticle ensemble based nanosensor via nanometal surface energy transfer," *Anal. Chem.*, vol. 83, no. 18, pp. 7061–7065, 2011.

[36] D. Y. Godovsky, "Device applications of polymer-nanocomposites," *Adv. Polym. Sci.*, vol. 165, pp. 163–205, 2000, Art. no. 153.

[37] N. N. Zhu, A. P. Zhang, Q. J. Wang, P. He, and Y. Z. Fang, "Lead sulfide nanoparticle as oligonucleotides labels for electrochemical stripping detection of DNA hybridization," *Eletroanalysis*, vol. 16, no. 7, pp. 577–582, 2004.

[38] J. J. Qiu, B. B. Weng, W. Y. Ge, L. L. McDowell, Z. H. Cai, and Z. S. Shi, "A broadband Pb-chalcogenide/CdS solar cells with tandem quantum-dots embedded in the bulk matrix (QDiM) absorption layers by using chemical bath deposition," *Sol. Energ. Mater. Sol. C.*, vol. 172, pp. 117–123, 2017.

[39] M. J. Speirs *et al.*, "Origin of the increased open circuit voltage in PbS-CdS core-shell quantum dot solar cells," *J. Mater. Chem. A*, vol. 3, no. 4, pp. 1450–1457, 2015.

[40] I. Kang and F. W. Wise, "Electronic structure and optical properties of PbS and PbSe quantum dots," *J. Opt. Soc. Am. B*, vol. 14, no. 7, pp. 1632–1646, 1997.

[41] J. Kuljanin, M. I. Čomor, V. Djoković, and J. M. Nedeljković, "Synthesis and characterization of nanocomposite of polyvinyl alcohol and lead sulfide nanoparticles," *Mater. Chem. Phys.*, vol. 95, no. 1, pp. 67–71, 2006.

[42] Y. W. Lee, C. M. Chen, C. W. Huang, S. K. Chen, and J. R. Jiang, "Passively Q-switched Er^{3+}-doped fiber lasers using colloidal PbS quantum dot saturable absorber," *Opt. Express*, vol. 24, no. 10, pp. 10675–10681, 2016.

[43] N. Ming *et al.*, "Mode-locked Er-doped fiber laser based on PbS/CdS core/shell quantum dots as saturable absorber," *Opt. Express*, vol. 26, no. 7, pp. 9017–9026, 2018.

[44] X. L. Sun *et al.*, "Stable passively Q-switched erbium-doped fiber laser incorporating a PbS quantum dots polystyrene composite film based saturable absorber," *Appl. Opt.*, vol. 57, no. 12, pp. 3231–3236, 2018.

[45] Y. Zhang *et al.*, "PbS nanoparticles for ultrashort pulse generation in optical communication region," *Part. Part. Syst. Char.*, vol. 35, no. 11, pp. 1–6, 2018, Art. no. 1800341.

[46] H. Y. Luo, J. F. Li, Y. Gao, Y. Xu, X. H. Li, and Y. Liu, "Tunable passively Q-switched Dy^{3+}-doped fiber laser from 2.71 to 3.08 μm using PbS nanoparticles," *Opt. Lett.*, vol. 44, no. 9, pp. 2322–2325, 2019.

[47] R. K Joshi, A. Kanjilal, and H. K. Sehgal, "Size dependence of optical properties in solution grown $Pb_{1-x}Fe_xS$ nanoparticle films," *Nanotechnology*, vol. 14, pp. 809–812, 2003.

[48] Y. Y. Feng, J. Zhang, P. Zhou, G. F. Luc, J.C. Bao, W. Wang, and Z. Xu, "A facile method to prepare PbS nanorods," *Mater. Res. Bull.*, vol. 39, pp. 1999–2005, 2004.

[49] M. S. Dhlamini *et al.*, "Photoluminescence properties of powder and pulsed laser-deposited PbS nanoparticles in SiO_2," *J. Lumin.*, vol. 128, pp. 1997–2003, 2008.

[50] J. Li *et al.*, "Thulium-doped all-fiber mode-locked laser based on NPR and 45°-tilted fiber grating," *Opt. Express*, vol. 22, no. 25, pp. 31020–31028, 2014.

[51] H. Zhang, D. Y. Tang, L. M. Zhao, and N. Xiang, "Coherent energy exchange between components of a vector soliton in fiber lasers," *Opt. Express*, vol. 16, no. 17, pp. 12618–12623, 2018.

[52] M. Pang, W. He, and P. S. J. Russell, "Gigahertz-repetition-rate Tm-doped fiber laser passively mode-locked by optoacoustic effects in nanobore photonic crystal fiber," *Opt. Lett.*, vol. 41, no. 19, pp. 4601–4604, 2016.

[53] M. Pang *et al.*, "Stable subpicosecond soliton fiber laser passively mode-locked by gigahertz acoustic resonance in photonic crystal fiber core," *Optica*, vol. 2, no. 4, pp. 339–342, 2015.

[54] C. Hönninger, R. Paschotta, F. Morier-Genoud, M. Moser, and U. Keller, "Q-switching stability limites of continuous-wave passive mode locking," *J. Opt. Soc. Am. B*, vol. 16, pp. 46–56, 1999.

[55] Q. Bao *et al.*, "Monolayer graphene as a saturable absorber in a mode-locked laser," *Nano Res.*, vol. 4, pp. 297–307, 2011.

[56] J. Z. Wang *et al.*, "152 fs nanotube-mode-locked thulium-doped all-fiber laser," *Sci. Rep.*, vol. 6, pp. 1–7, 2016, Art. no. 28885.

[57] Z. Q. Wang *et al.*, "Passively Q-switched Er-doped fiber Lasers using alcohol," *J. Lightw. Technol.*, vol. 33, no. 23, pp. 4857–4861, 2015.

[58] Z. Q. Wang *et al.*, "Self-starting ultrafast fiber lasers mode-locked with alcohol," *Opt. Lett.*, vol. 40, no. 16, pp. 3699–3672, 2015.

[59] W. B. Cho *et al.*, "Passive mode-locking of a Tm-doped bulk laser near 2 μm using a carbon nanotube saturable absorber," *Opt. Express*, vol. 17, no. 13, pp. 11007–11012, 2009.

[60] D. I. M. Zen *et al.*, "Mode-locked thulium-bismuth co-doped fiber laser using graphene saturable absorber in ring cavity," *Appl. Opt.*, vol. 52, no. 6, pp. 1226–1229, 2013.

[61] J. Sotor, G. Sobon, I. Pasternak, A. Krajewska, W. Strupinski, and K. M. Abramski, "Simultaneous mode-locking at 1565 nm and 1944 nm in fiber laser based on common graphene saturable absorber," *Opt. Express*, vol. 21, no. 16, pp. 18994–19002, 2013.

[62] G. Sobon, J. Sotor, I. Pasternak, A. Krajewska, W. Strupinski, and K. M. Abramski, "Thulium-doped all-fiber laser mode-locked by CVD-graphene/PMMA saturable absorber," *Opt. Express*, vol. 21, no. 10, pp. 127971–127976, 2013.

[63] B. Fu, Yi Hua, X. S. Xiao, H. W. Zhu, Z. P. Sun, and C. X. Yang, "Broadband graphene saturable absorber for pulsed fiber lasers at 1, 1.5, and 2 μm," *IEEE J. Sel. Top. Quant. Electron.*, vol. 20, no. 5, pp. 411–415, 2014.

[64] Q. Wang, T. Chen, B. Zhang, M. Li, Y. Lu, and K. P. Chen, "All-fiber passively mode-locked thulium-doped fiber ring laser using optically deposited graphene saturable absorbers," *Appl. Phys. Lett.*, vol. 102, pp. 1–5, 2013, Art. no. 131117.

[65] H. Li, J. Liu, Z. Cheng, J. Xu, F. Tan, and P. Wang, "Pulse-shaping mechanisms in passively mode-locked thulium-doped fiber lasers," *Opt. Express*, vol. 23, no. 5, pp. 6292–6303, 2015.

[66] M. Jung, J. Lee, J. Park, J. Koo, Y. M. Jhon, and J. H. Lee, "Mode-locked, 1.94 μm, all-fiberized laser using WS_2-based evanescent field interaction," *Opt. Express*, vol. 23, no. 15, pp. 19996–20006, 2015.

[67] L. M. Cao, X. Li, R. Zhang, D. D. Wu, and S. X. Dai, "Tm-doped fiber laser mode-locking with MoS_2-polyvinyl alcohol saturable absorber," *Opt. Fiber Technol.*, vol. 48, pp. 187–192, 2018.

[68] J. Lee, J. Koo, J. Lee, Y. M. Jhon, and J. H. Lee, "All-fiberized, femtosecond laser at 1912 nm using a bulk-like $MoSe_2$ saturable absorber," *Opt. Mater. Express*, vol. 7, no. 1912, pp. 2968–2979, 2017.

[69] J. Wang *et al.*, "Ultrafast thulium-doped fiber laser mode locked by monolayer WSe_2," *IEEE J. Sel. Top. Quant. Electron.*, vol. 24, no. 3, pp. 1–6, 2018, Art. no. 1100706.

[70] J. Wang *et al.*, "Mode-locked thulium-doped fiber laser with chemical vapor deposited molybdenum ditelluride," *Opt. Lett.*, vol. 43, no. 9, pp. 1998–2001, 2018.